

# Magnetically Recoverable Nanoflake-Shaped Iron Oxide/Pt Heterogeneous Catalysts and Their Excellent Catalytic Performance in the Hydrogenation Reaction

Yanping Liu,<sup>†,||</sup> Jooyoung Chung,<sup>§,||</sup> Youngjin Jang,<sup>‡</sup> Shuai Mao,<sup>†</sup> B. Moon Kim,<sup>§</sup> Yongqiang Wang,<sup>†</sup> and Xiaohui Guo<sup>\*,†</sup>

<sup>†</sup>Key Lab of Synthetic and Natural Functional Molecule Chemistry of Ministry of Education, and the College of Chemistry and Materials Science, Northwest University, Xi'an 710069, P. R. China.

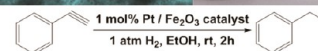
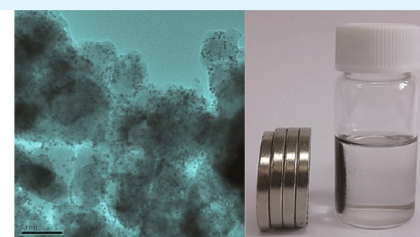
<sup>‡</sup>School of Chemical and Biological Engineering, Seoul National University, Seoul, Korea

<sup>§</sup>Department of Chemistry, Seoul National University, Seoul, Korea

## S Supporting Information

**ABSTRACT:** In this study, a kind of unique Fe<sub>2</sub>O<sub>3</sub>/Pt hybrid consisting of uniform platinum nanoparticles deposited on a nanoflake-shaped Fe<sub>2</sub>O<sub>3</sub> support was prepared by using a solvothermal reaction followed by a heat-induced reduction process. The prepared Fe<sub>2</sub>O<sub>3</sub> sample displays well-defined nanoflake-like morphology; remarkably, there are many specific cavities on its surface. In addition, uniform Pt nanoparticles with narrow size distribution were deposited onto the surface of the preformed flake-like Fe<sub>2</sub>O<sub>3</sub> support to form the Fe<sub>2</sub>O<sub>3</sub>/Pt hybrid via a facile heat-induced reduction reaction. Thus, the prepared Fe<sub>2</sub>O<sub>3</sub>/Pt hybrid can serve as heterogeneous catalyst over the hydrogenation reaction. Results demonstrated that the specific Fe<sub>2</sub>O<sub>3</sub>/Pt heterogeneous catalyst exhibits good catalytic performances, including high conversion, specific selectivity, and excellent recycling durability, over hydrogenation reactions for different substrates. Furthermore, the prepared Fe<sub>2</sub>O<sub>3</sub>/Pt heterogeneous catalyst could be easily separated from the product mixture by using a magnet and could be recycled for 10 cycles without catalytic activity loss. In a word, the present synthetic approach is facile, scalable, and reproducible, which can be easily facilitated to prepare other types of noble metals/metal oxide composite systems.

**KEYWORDS:** iron oxide, Pt nanoparticle, flake-like, heterogeneous catalyst, hydrogenation



Run	1st	2nd	3rd	4th	5th	6th	7th	8th	9th	10th
Yield (%)	99	99	99	99	99	99	99	99	99	99

## INTRODUCTION

Developing nanoparticle (NPs) catalysts with controlled size and surface textures is critical to achieving desirable catalytic performances.<sup>1–4</sup> Of numerous NP catalyst systems, platinum (Pt) NPs have attracted particular interest due to their superior catalytic performances in many chemical reactions,<sup>5–9</sup> especially in hydrogen oxidation<sup>10–14</sup> and oxygen reduction in catalytic applications.<sup>14–17</sup> However, the need to limit Pt usage has greatly promoted the search for Pt-based heterogeneous catalysts with high activity or for non-Pt composite catalysts with comparable catalytic properties.

As we all know, Pt NPs always serve as excellent and versatile catalysts in various important reactions but occur at very low levels of abundance in nature.<sup>18,19</sup> Therefore, further enhancement of their utilization efficiency, catalytic activity, and recycle durability has long been of fundamental importance. According to previous study results, it was found that utilizing controlled solution synthetic approaches can give rise to metal oxides/Pt composite catalysts and exhibit improved catalytic performances compared with pure Pt species.<sup>20–23</sup>

It should be noted that magnetically separable composites as highly durable catalysts have attracted increasing attention due to their scientific and technological importance.<sup>4,24</sup> Magnetic substrate supported catalysts can be quickly recovered with an external magnet due to the paramagnetic character of the support, resulting in remarkable catalyst recovery without using complicated filtration/separation processes.<sup>25,26</sup> This could greatly enhance the catalytic efficiency and therefore effectively decrease operation costs, which is essential for practical applications. As a result, developing a kind of magnetically recoverable Pt based composite catalyst would highlight their great advantages in future industry applications. Consequently, regarding the study of magnetically separate Pt based composite catalysts has triggered great interest and made some progress recently. Especially, Liang et al. prepared partially reduced Pt/ $\gamma$ -Fe<sub>2</sub>O<sub>3</sub> magnetic composite catalysts that exhibit good catalytic properties in the selective hydro-

Received: November 4, 2013

Accepted: December 26, 2013

Published: December 26, 2013

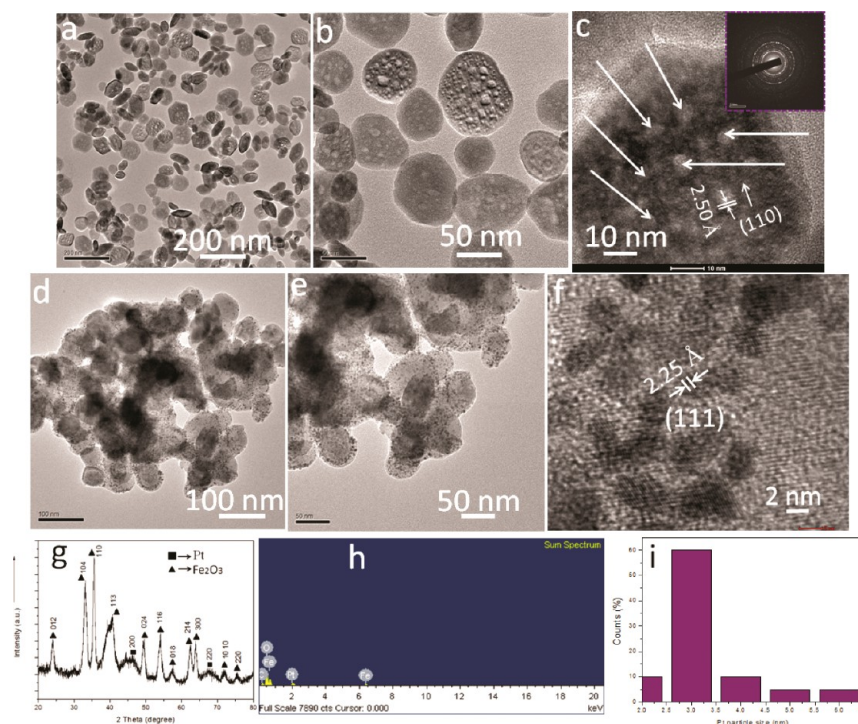


**Figure 1.** Morphology, structure, and component analysis for the prepared iron oxide based samples. (a–c) SEM and TEM images of the Fe<sub>2</sub>O<sub>3</sub> nanoplate; (d–f) TEM images of the nanoflake-like Fe<sub>2</sub>O<sub>3</sub>/Pt hybrid; (g) XRD pattern for the Fe<sub>2</sub>O<sub>3</sub>/Pt sample; (h) EDS pattern of the Fe<sub>2</sub>O<sub>3</sub>/Pt hybrid; (i) size distribution curve of Pt NPs.

generation of 2,4-dinitrochlorobenzene and iodonitrobenzenes.<sup>27</sup> Previous literature reported that the Pd/Fe<sub>3</sub>O<sub>4</sub> composite catalyst can be prepared via the one-pot template-free synthetic route and displays high catalytic activity over the hydrogenation reaction.<sup>28</sup> More interestingly, a kind of novel magnetic Pt/SiO<sub>2</sub>/Fe<sub>3</sub>O<sub>4</sub> composite catalyst was prepared via the simple solution approach, which exhibits better catalytic performances over the enantioselective hydrogenation of various activated ketones.<sup>29</sup> However, to the best of our knowledge, the synthesis of unique nanoflake-like iron oxide supported Pt based heterogeneous catalysts has rarely been reported. Hence, the construction of or exploring the catalytic performances of the magnetically separable heterogeneous catalyst would be highly expected for the development of this field.

In this study, we present the synthesis of a class of novel magnetically recoverable nanoflake-like iron oxide/Pt hybrids via two-step solution reaction processes. The iron oxide/Pt hybrid materials serve as catalysts in hydrogenation reactions, and we systematically explore their catalytic performances, including conversion, selectivity, and recycling durability. Herein, it was believed that the specific synthetic approach could provide a promising avenue for the preparation of other noble metal-based heterogeneous catalysts with unique morphologies and surface textures.

## EXPERIMENTAL SECTION

**Preparation of Nanoflake-Like Fe<sub>2</sub>O<sub>3</sub>.** All chemicals are commercially available and were used without further purification. Iron(II) acetylacetonat (99.95% purity) and potassium platinumchloride (99.9% purity) were purchased from Sigma-Aldrich Company. Polyvinylpyrrolidone (PVP) (*M<sub>w</sub>* ~10000) was purchased from Sinopharm Chemical Reagent Company.

In a typical synthesis, first, 0.15 g of iron(II) acetylacetonat (Fe(acac)<sub>2</sub>) was added into a solution containing 5 mL of deionized water (DIW) and 25 mL of *N,N*-dimethylformamide (DMF), and the

mixture solution was magnetically stirred for 0.5 h. Next, the resultant homogeneous solution was transferred into a 50 mL Teflon-lined autoclave and then maintained at 120 °C in an oven for 18 h. After that, the prepared products were collected and washed with DIW and absolute ethanol several times and finally dried in a 60 °C oven for 8 h.

**Synthesis of the Fe<sub>2</sub>O<sub>3</sub>/Pt Heterogeneous Catalyst.** For the synthesis of the Fe<sub>2</sub>O<sub>3</sub>/Pt sample, first the potassium platinumchloride (K<sub>2</sub>PtCl<sub>4</sub>) precursor solution was prepared by dissolving 0.02 g of K<sub>2</sub>PtCl<sub>4</sub> in 2 mL of ethylene glycol (EG) in a glass vial. Meanwhile, polyvinylpyrrolidone (PVP) (*M<sub>w</sub>* ~10000) was dissolved in 2 mL of EG solvent. Consequently, 50 mg of Fe<sub>2</sub>O<sub>3</sub> solution including 15 mL of EG was placed into a 50 mL round-bottomed glass flask and then ultrasonication performed for 10 min. Next, the resulting homogeneous solution was heated in a 100 °C oil bath under magnetic stirring interaction. After stirring for 1 h, the above two prepared solutions were simultaneously injected into the round-bottomed glass flask drop by drop. The resulting solution was further processed at 100 °C for an additional 22 h. Afterward, the resultant sample can be retrieved via centrifugation and washing with absolute ethanol. Finally, the product was obtained via drying in a 60 °C oven for 8 h.

**Characterization.** The powder X-ray diffraction (XRD) measurement was performed using a Rigaku D/Max-3C diffractometer (Cu K $\alpha$  radiation,  $\lambda = 0.15418$  nm). Fourier transform infrared spectroscopy (FTIR) was recorded via a Bruker EQUINOX-55 infrared spectrophotometer on a KBr pellet. Sample images were recorded via field emission scanning electron microscopy (FESEM) (JEOL, JSM-6701, Japan) with an operating voltage of 20 kV. Transmission electron microscopy (TEM) images were obtained on a microscope (Philips Tecnai G2 F20) at 200 kV. The sample for TEM measurement was suspended in ethanol and thus supported onto a copper grid including a holey carbon film. The X-ray photoelectron spectroscopy (XPS) experiments were performed in an ultrahigh vacuum (UHV) multipurpose surface analysis system (SIGMA PROBE, Thermo, UK) operating at base pressures <10<sup>-10</sup> mbar.

**Catalytic Performance Measurement.** In a typical catalytic testing, 0.5 mmol of the prepared Fe<sub>2</sub>O<sub>3</sub>/Pt sample was dissolved in 4 mL of ethanol with 1 mol % of catalyst under 1 atm H<sub>2</sub> atmosphere. The reaction process was monitored by flash column chromatography.

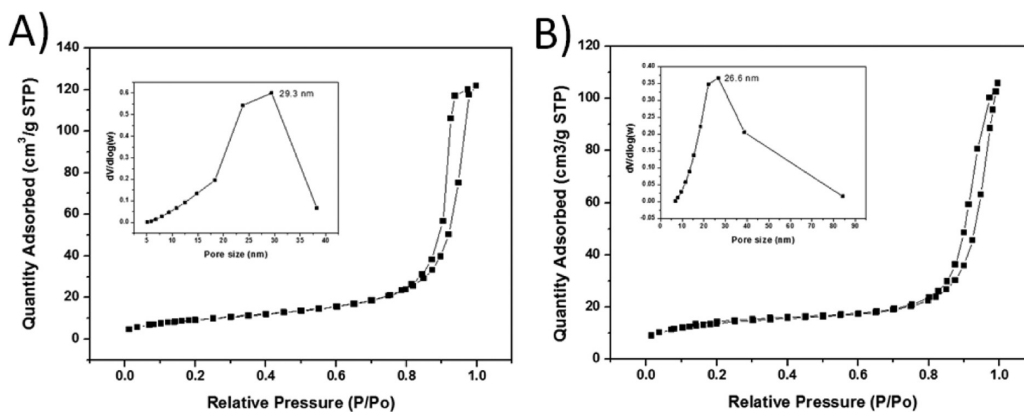


**Figure 2.** Isothermal N<sub>2</sub> adsorption–desorption curves and pore size-distribution curves (insets) for the prepared samples. (A) Pure nanoflake-like Fe<sub>2</sub>O<sub>3</sub> and (B) Fe<sub>2</sub>O<sub>3</sub>/Pt.

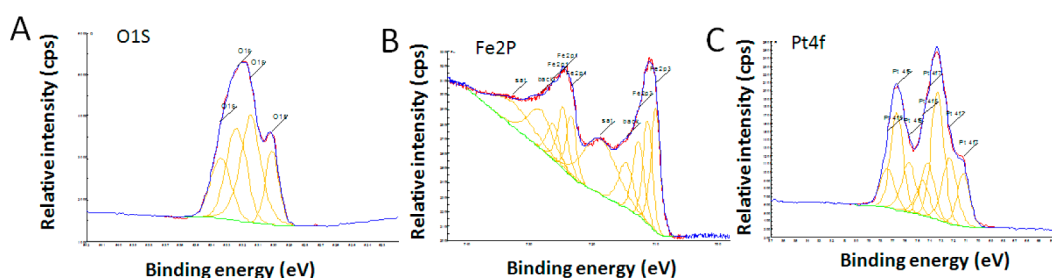


**Figure 3.** XPS spectrum for the prepared Fe<sub>2</sub>O<sub>3</sub>/Pt hybrid sample. (A) O1s; (B) Fe2p; (C) Pt4f.

The reaction mixture was stirred at room temperature for several hours. After the reaction, the catalyst was separated by a small magnet placed at the bottom of the reaction vessel, and the conversion was estimated by gas chromatography (P.E. AutoSystem XL). After that, the catalyst was washed with absolute ethanol three times, and then dried at room temperature for the next cycle. The catalytic reactions were then repeated, and even after 5 cycles, there was no deterioration in the catalytic efficiency. The extracted residue was directly analyzed with gas chromatography or purified by flash column chromatography to yield the desired product.

## RESULTS AND DISCUSSION

Herein, a kind of unique flake-shape sample with uniform size was prepared via a simple hydrothermal process, as shown in Figure 1a–c. It can be found that the prepared sample exhibits irregular flake-like structure with a mean length of 50 nm. Remarkably, it was seen that there are many cavities on its surface, as clearly indicated by white arrows in Figure 1c. The obtained sample was indexed to be cubic-phase Fe<sub>2</sub>O<sub>3</sub> structure according to JCPDS card no. 39-1346 (Figure 1g). In addition, further TEM images reveal that the prepared Fe<sub>2</sub>O<sub>3</sub> sample displays a well-defined crystal lattice stripe with a spacing of ~2.50 Å, corresponding to the (110) plane (Figure 1c). Moreover, a kind of iron oxide-based hybrid structure was observed. As shown in Figure 1d, the smaller NPs deposited on the surface of the iron oxide support can be assigned to be face-centered cubic Pt according to the standard JCPDS card no. 87-0642. No impurity peaks were detected in the XRD pattern (Figure 1g). Clearly, Fe<sub>2</sub>O<sub>3</sub>/Pt hybrids actually do consist of flake-shaped Fe<sub>2</sub>O<sub>3</sub> and numerous Pt NPs with an average size that ranged from 3 to 6 nm; in addition, the HRTEM image finds that the Pt NPs display a well-resolved crystal lattice stripe. The spacing was measured to be 2.25 Å, corresponding to the (111) plane, as shown in Figure 1f. It was observed that

Pt NPs are well-dispersed on the surface of flake-like Fe<sub>2</sub>O<sub>3</sub> and found to be narrow in size distribution (Figure 1i). This demonstrated that Pt NPs were successfully immobilized onto the surface of the flake-like iron oxide support. Moreover, the energy dispersive spectroscopy (EDS) pattern can further identify the presence of Fe, O, and Pt elements of the prepared sample (Figure 1h).

The isothermal N<sub>2</sub> adsorption–desorption analysis was performed to further evaluate the porous features for the prepared samples; the results are shown in Figure 2. The data show that the isothermal nitrogen adsorption curves are typical IV-type curves. The loop nature of the nitrogen adsorption isotherm suggests a uniform mesoporous feature. Additionally, the specific BET surface areas for the prepared nanoflake-like Fe<sub>2</sub>O<sub>3</sub> and Fe<sub>2</sub>O<sub>3</sub>/Pt samples are measured to be 34.195 and 45.573 m<sup>2</sup> g<sup>-1</sup>, respectively. In addition, according to the corresponding Barrett–Joyner–Halenda (BJH) pore size distribution curve, their pore sizes are measured to be 29.3 and 26.6 nm, respectively (insets in Figure 2).

In order to investigate the element complex state of the samples, X-ray photoelectron spectroscopy (XPS) was performed on the samples, as shown in Figure 3. The XPS spectrum in Figure 3A indicates the characteristic peak of O1s centered at approximately 531 eV. XPS spectrum of Fe2p (Figure 3B) shows two characteristic peaks that centered at approximately 724.4 and 709.7 eV, which can be attributed to Fe2p<sub>1/2</sub> and Fe2p<sub>3/2</sub>, respectively,<sup>30,31</sup> indicating the presence of Fe<sup>3+</sup> species. A representative high-resolution Pt 4f spectrum is shown in Figure 3C. Two well-resolved Pt 4f<sub>7/2</sub> and Pt 4f<sub>5/2</sub> peaks are observed at approximately 73.1 and 76.3 eV respectively, in particular, the two binding energies of Pt 4f<sub>7/2</sub> and 4f<sub>5/2</sub> correspond well to zero valent state Pt species.<sup>32–34</sup> More interestingly, it was found from XPS spectra of Pt 4f<sub>7/2</sub> that the binding energy of the Pt 4f<sub>7/2</sub> in Fe<sub>2</sub>O<sub>3</sub>/Pt has a high value

of 73.1 eV, 1.6 eV higher than that of most previously reported Pt NPs (c.a. 71.5 eV).<sup>35</sup> This provides evidence of an electron transfer from the Pt NPs to iron cation or the iron oxide component, hence producing the specific Pt–O coordination complex form in the present Fe<sub>2</sub>O<sub>3</sub>/Pt system.

Furthermore, FTIR testing was performed to explore the structural features for the prepared samples; results are shown in Figure 4. Figure 4a shows the FTIR spectrum of pure flake-

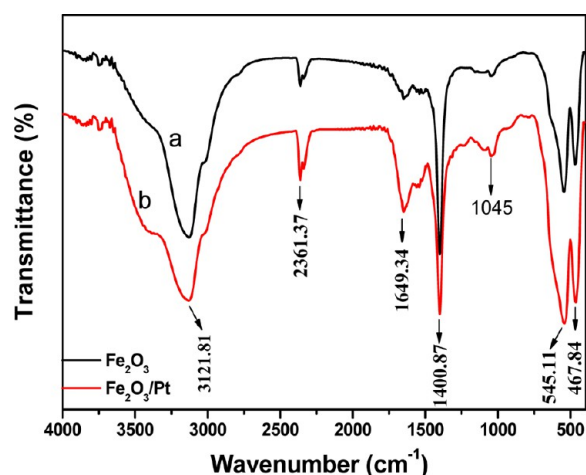
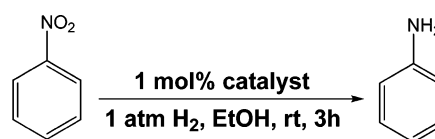


**Figure 4.** FTIR spectrum of the iron oxide-based samples. (a) Flake-like Fe<sub>2</sub>O<sub>3</sub>; (b) Fe<sub>2</sub>O<sub>3</sub>/Pt hybrids.

like Fe<sub>2</sub>O<sub>3</sub>. It was observed that the peak at approximately 3121 cm<sup>-1</sup> corresponds to the  $\nu(\text{O-H})$  stretching vibration mode. The well-resolved band at approximately 2361 cm<sup>-1</sup> was assigned to the asymmetric stretching mode of the C–H group. Additionally, the peaks centered at approximately 1649, 1400, and 1045 cm<sup>-1</sup> can be assigned to C=O, C=C, and C–C stretching vibration modes of the acetylacetonate molecule, respectively.<sup>36</sup> The strong peaks at 545 and 468 cm<sup>-1</sup> correspond to Fe–O bond vibration modes.<sup>37</sup> The FTIR spectrum of the Fe<sub>2</sub>O<sub>3</sub>/Pt hybrid sample is almost identical to the case of the pure Fe<sub>2</sub>O<sub>3</sub> system, even the immobilization of Pt NPs on the surface of the flake-like iron oxide support. The result is shown in Figure 4b.

Recently, various kinds of Pt-based composites have been tested as catalysts toward the reduction of nitrobenzene in the presence of hydrazine. We tested the catalytic activity of the prepared Fe<sub>2</sub>O<sub>3</sub>/Pt over the hydrogenation reaction. It was found that the whole reduction reaction was almost finished within 3 h and exclusively yielding aniline. Remarkably, the Fe<sub>2</sub>O<sub>3</sub>/Pt hybrid catalyst exhibits a high conversion of ~95% after one cycle reaction. In addition, it still has high reuse capability after 10 cycles over the dehydrogenation catalytic reaction (Table 1 and Figure 5). Meanwhile, for comparison, different types of catalysts were used for the reduction reaction of nitrobenzene. Results are shown in Table 1. It was clearly seen that the prepared Fe<sub>2</sub>O<sub>3</sub>/Pt catalyst exhibits superior catalytic activity compared to that of other three catalysts. Similarly, further decreasing the loading amount of Pt species to 60% (weight percentage relative to the prepared Fe<sub>2</sub>O<sub>3</sub>/Pt) to prepare the Fe<sub>2</sub>O<sub>3</sub>/Pt catalyst, we observed that the specific catalyst can maintain high conversion of ~95% after 8 cycles in nitrobenzene hydrogenation reaction, indicating excellent recycling durability (Figure S1, Supporting Information). As a result, it was speculated that this case is probably due to the

**Table 1.** Catalytic Activity Comparison of Different Catalysts over Nitrobenzene Hydrogenation Reaction<sup>a</sup>



entry	catalysts	time (h)	yield (%)
1	Fe <sub>2</sub> O <sub>3</sub> /Pt	3	95
2	Pt	3	90
3	Pd/C	3	92
4	Fe <sub>2</sub> O <sub>3</sub>	3	0

<sup>a</sup>All catalytic reactions were performed at room temperature.

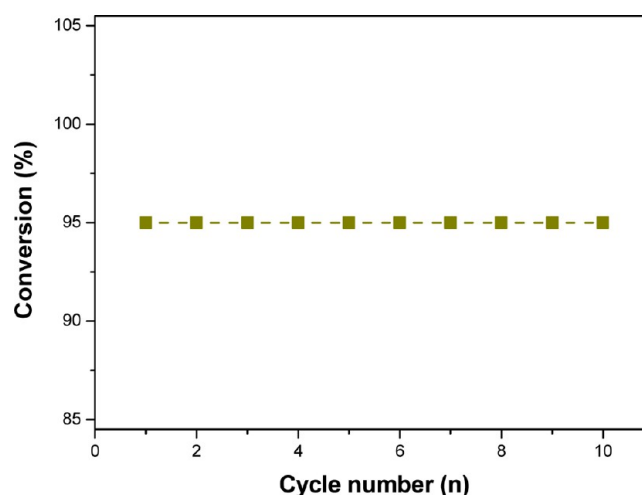


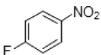
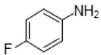
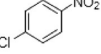
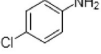
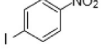
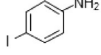
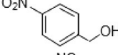
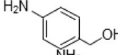
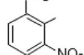
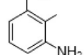
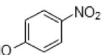
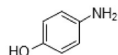
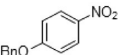
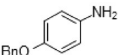
**Figure 5.** Recycling catalytic curves when using Fe<sub>2</sub>O<sub>3</sub>/Pt as the catalyst over the hydrogenation reaction for the nitrobenzene substrate.

high accessible surface area and specific surface defects from iron oxide, as well as the smaller size of active Pt species.<sup>2</sup>

Furthermore, to examine the scope of the reduction reaction using the Fe<sub>2</sub>O<sub>3</sub>/Pt heterogeneous catalyst, the catalytic activity of the prepared Fe<sub>2</sub>O<sub>3</sub>/Pt catalyst was tested over hydrogenation for a variety of nitro and unsaturated compounds to their corresponding products. Detailed results for all the catalytic reactions are given in Table 2. It was found that most of the hydrogenation reaction was completed within 3 h. Results demonstrated that the Fe<sub>2</sub>O<sub>3</sub>/Pt catalyst displays high catalytic activity for the aromatic nitro and unsaturated compound substrates, in which the nitro groups of nitroarenes with different functional groups was selectively reduced to the amino moiety. In particular, a satisfactory yield (99%) still remained after processing several cycles. The recyclability of the catalyst could be attributed to the efficient stabilization of the active Pt species by the amine groups on the iron oxide surface.<sup>35</sup> In contrast, entry 7 was used as the catalytic substrate; it requires at least 5 h to complete the reaction under similar catalytic conditions, which is probably due to the relatively large steric hindrance of the reaction substrate.<sup>28</sup>

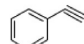
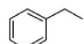
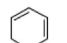
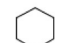
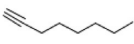
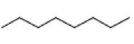
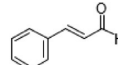
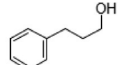
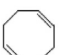
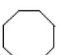
Furthermore, the catalytic performance of Fe<sub>2</sub>O<sub>3</sub>/Pt for phenylacetylene was performed. The hydrogenation reaction was completed within 2 h, and the alkynyl group was selectively reduced to the alkyl group with a conversion of 100% (Table 3). The catalyst exhibits high chemoselectivity in the reduction of the triple bond, especially for cinnamaldehyde and 1,5-

**Table 2. Catalytic Feature Summary of the Hydrogenation Reaction for Various Substituted Nitrobenzenes<sup>a</sup>**

Entry	Substrate	Product	Time (h)	Yield (%)
1			3	99
2			3	99
3			3	99
4			3	99
5			3	99
6			2	99
7			5	99

<sup>a</sup>Herein, Fe<sub>2</sub>O<sub>3</sub>/Pt serves as the catalyst at room temperature. Experimental conditions: substrate = 0.5 mmol, H<sub>2</sub> = 1 atm, the catalyst = 1 mol %, and solvent = 4 mL of EtOH at RT.

**Table 3. Catalytic Activity Summary of the Hydrogenation Reaction for Phenylacetylene and Substituted Compounds<sup>a</sup>**

Entry	Substrate	Product	Time (h)	Yield (%)
1			2	100
2			3	99
3			2	99
4			24	93
5			24	63

<sup>a</sup>Herein, Fe<sub>2</sub>O<sub>3</sub>/Pt serves as the catalyst, and the catalytic reaction was performed at room temperature. Experimental conditions: substrate = 0.5 mmol, H<sub>2</sub> = 1 atm, the catalyst = 1 mol %, and solvent = 4 mL of EtOH at RT.

cyclooctadiene (Table 3, entries 4–5). Their conversions are 93 and 63%, respectively. Herein, it was inferred that the weakened electronic back-donation feedback from Pt NPs to the aromatic ring would indeed weaken the electrophilic attack of the cleaved hydrogen atoms on the adsorbed aromatic ring, therefore lowering the conversion of the reaction substrate; the case was well demonstrated in previously reported results.<sup>35,38,39</sup>

**Table 4. Recycling Catalytic Summary of the Hydrogenation Reaction for the Phenylacetylene Substrate<sup>a</sup>**

run	1st	2nd	3rd	4th	5th	6th	7th	8th	9th	10th
yield (%)	99	99	99	99	99	99	99	99	99	99

<sup>a</sup>Herein, Fe<sub>2</sub>O<sub>3</sub>/Pt serves as the catalyst, and the catalytic reaction was performed at room temperature.

Meanwhile, the catalytic durability of the Fe<sub>2</sub>O<sub>3</sub>/Pt catalyst was investigated for the phenylacetylene substrate. The result indicates that the conversion of phenylacetylene still remains at 99% even after 10 cycles (Table 4), implying outstanding durability of the Fe<sub>2</sub>O<sub>3</sub>/Pt catalyst. When the recycling catalytic reaction was completed, the Fe<sub>2</sub>O<sub>3</sub>/Pt heterogeneous catalyst could be easily separated from the reaction mixture using a magnet (Figure 6a), and the morphology and structure of the

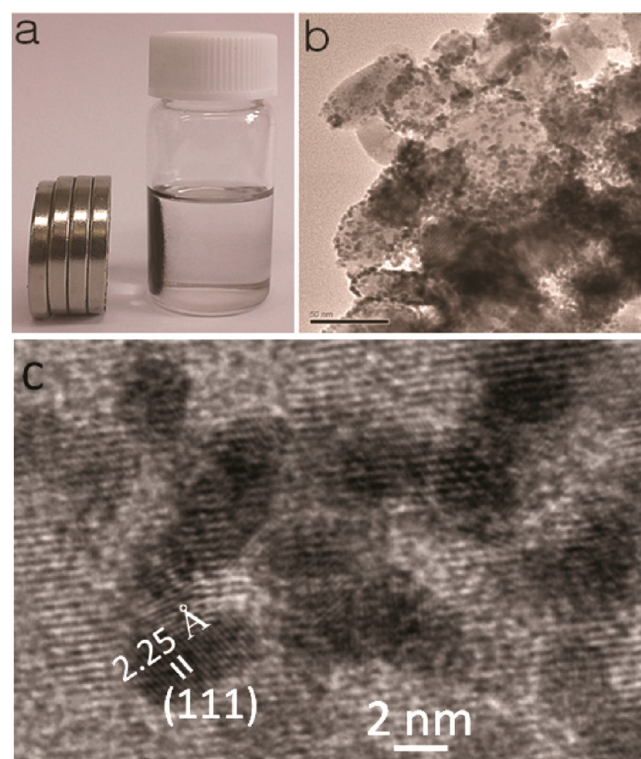


**Figure 6.** Photographs of the magnetically separable Fe<sub>2</sub>O<sub>3</sub>/Pt catalyst (a); TEM image (b); and the HRTEM image of the Fe<sub>2</sub>O<sub>3</sub>/Pt catalyst after undergoing 10 catalytic cycles (c).

Fe<sub>2</sub>O<sub>3</sub>/Pt catalyst do not occur change, as shown in Figures 6b and c. Additionally, the recycled catalyst can still maintain the same crystal structure with the Fe<sub>2</sub>O<sub>3</sub>/Pt before catalytic reaction, as shown in Figure S2, Supporting Information, implying their high structural stability. Also, it was found that the Pt NPs were well dispersed on the surface of the Fe<sub>2</sub>O<sub>3</sub> support. After washing with ethanol to remove the adsorbed purities, the recovered catalyst was reused in the next cycle catalytic reaction. The recovered Fe<sub>2</sub>O<sub>3</sub>/Pt catalyst does not undergo catalytic activity loss over 10 cycles; this clearly indicated that Pt species leaching was negligible.

## CONCLUSIONS

In summary, we have demonstrated a simple synthetic route for the synthesis of magnetically recoverable flake-like Fe<sub>2</sub>O<sub>3</sub>/Pt heterogeneous catalysts. Catalytic results demonstrated that the resultant Fe<sub>2</sub>O<sub>3</sub>/Pt heterogeneous catalyst displays high catalytic activity, low cost, long-term stability, and easy recovery. More interestingly, these encouraging findings could be expanded to other reaction systems and could open up a new direction in catalysis and energy-related fields.

## ASSOCIATED CONTENT

### Supporting Information

Recycling catalytic summary of the hydrogenation reaction for the nitrobenzene substrate and the XRD pattern of the prepared Fe<sub>2</sub>O<sub>3</sub>/Pt hybrid catalyst after the dehydrogenation catalysis reaction. This material is available free of charge via the Internet at <http://pubs.acs.org>.

## AUTHOR INFORMATION

### Corresponding Author

\*Tel: +86-29-88302604. E-mail: [guoxh2009@nwu.edu.cn](mailto:guoxh2009@nwu.edu.cn).

### Author Contributions

<sup>†</sup>Y.L. and J.C. equally contributed to this work.

### Notes

The authors declare no competing financial interest.

## ACKNOWLEDGMENTS

We acknowledge funding support from the National Science Foundation of China (NSFC) (numbers 21001087, 21173167, and J1210057), the Education committee of Shannxi Province (grant numbers 2010JK870 and 2010JS115), and the Program for New Century Excellent Talents in University (NCET-13-0953).

## REFERENCES

- (1) Lee, E. P.; Peng, Z.; Cate, D. M.; Yang, H.; Campbell, C. T.; Xia, Y. *J. Am. Chem. Soc.* **2007**, *129*, 10634–10635.
- (2) Rioux, R. M.; Song, H.; Grass, M.; Habas, S.; Niesz, K.; Hoefelmeyer, J. D.; Yang, P.; Somorjai, G. A. *Top. Catal.* **2006**, *39*, 167–174.
- (3) Mori, K.; Hara, T.; Mizugaki, T.; Ebitani, K.; Kaneda, K. *J. Am. Chem. Soc.* **2004**, *126*, 10657–10666.
- (4) Wittmann, S.; Schatz, A.; Grass, R. N.; Stark, W. J.; Reiser, O. *Angew. Chem., Int. Ed.* **2010**, *49*, 1867–1870.
- (5) Teng, X. W.; Liang, X. Y.; Maksimuk, S.; Yang, H. *Small* **2006**, *2*, 249–253.
- (6) Coombs, J. R.; Haeflner, F.; Kliman, L. T.; Morken, J. P. *J. Am. Chem. Soc.* **2013**, *135*, 11222–11231.
- (7) Yang, M.; Somorjai, G. A. *J. Am. Chem. Soc.* **2003**, *125*, 11131–11135.
- (8) Jang, Y.; Chung, J.; Kim, S.; Jun, S. W.; Kim, B. H.; Lee, D. W.; Kim, B. M.; Hyeon, T. *Phys. Chem. Chem. Phys.* **2011**, *13*, 2512–2516.
- (9) Lee, E. P.; Peng, Z.; Chen, W.; Chen, S.; Yang, H.; Xia, Y. *ACS Nano* **2008**, *2*, 2167–2173.
- (10) Mori, K.; Yoshioka, N.; Kondo, Y.; Takeuchi, T.; Yamashita, H. *Green Chem.* **2009**, *11*, 1337–1342.
- (11) Bratlie, K. M.; Montano, M. O.; Flores, L. D.; Paajanen, M.; Somorjai, G. A. *J. Am. Chem. Soc.* **2006**, *128*, 12810–12816.
- (12) Lu, Y.; Zhu, H.; Li, W.; Hu, B.; Yu, S. *J. Mater. Chem. A* **2013**, *1*, 3783–3788.
- (13) Rhee, C. K.; Kim, B. J.; Ham, C.; Kim, Y.-J.; Song, K.; Kwon, K. *Langmuir* **2009**, *25*, 7140–7147.

- (14) (a) Tiwari, J. W.; Tiwari, R. N.; Singh, G.; Kim, K. S. *Nano Energy* **2013**, *2*, 553–578. (b) Tiwari, J. N.; Tiwari, R. N.; Kim, K. S. *Prog. Mater. Sci.* **2012**, *57*, 724–803.
- (15) Wang, C.; Daimon, H.; Lee, Y.; Kim, J.; Sun, S. *J. Am. Chem. Soc.* **2007**, *129*, 6974–6975.
- (16) Wang, C.; Daimon, H.; Onodera, T.; Koda, T.; Sun, S. *Angew. Chem., Int. Ed.* **2008**, *47*, 3588–3591.
- (17) Antolini, E. *Energy Environ. Sci.* **2009**, *2*, 915–931.
- (18) Polshettiwar, V.; Luque, R.; Fihri, A.; Zhu, H.; Bouhrara, M.; Basset, J. M. *Chem. Rev.* **2011**, *111*, 3036–3075.
- (19) Poliakov, M.; Fitzpatrick, J. M.; Farren, T. R.; Anastas, P. T. *Science* **2002**, *297*, 807–810.
- (20) Hara, T.; Kaneta, T.; Mori, K.; Mitsudome, T.; Mizugake, T.; Ebitani, K.; Kaneda, K. *Green Chem.* **2007**, *9*, 1246–1251.
- (21) Fu, Q.; Li, W. X.; Yao, Y.; Liu, H. Y.; Su, H.; Ma, D.; Gu, X.; Chen, L.; Wang, Z.; Zhang, H.; Wang, B.; Bao, X. H. *Science* **2010**, *328*, 1141–1144.
- (22) Wang, C.; Daimon, H.; Sun, S. *Nano Lett.* **2009**, *9*, 1493–1496.
- (23) Barmatova, M. V.; Ivanchikova, I. D.; Kholdeeva, O. A.; Shmakov, A. N.; Zaikovskii, V. I.; Mel'gunov, M. S. *J. Mater. Chem.* **2009**, *19*, 7332–7339.
- (24) Yoon, H.; Ko, S.; Jang, J. *Chem. Commun.* **2007**, *14*, 1468–1470.
- (25) Ma, Y.; Yue, B.; Yu, L.; Wang, X.; Hu, Z.; Fan, Y.; Che, Y. *J. Phys. Chem. C* **2008**, *112*, 472–475.
- (26) Jang, Y.; Kim, S.; Jun, W.; Kim, B. H.; Hwang, S.; Song, I. K.; Kim, B. M.; Hyeon, T. *Chem. Commun.* **2011**, *47*, 3601–3603.
- (27) Liang, M. H.; Wang, X. D.; Liu, H. Q.; Liu, H. C.; Wang, Y. J. *Catal.* **2008**, *255*, 335–342.
- (28) Zhang, F.; Jin, J.; Zhong, X.; Li, S.; Niu, J.; Ma, J. *Green Chem.* **2011**, *13*, 1238–1243.
- (29) Panella, B.; Vargas, A.; Baiker, A. *J. Catal.* **2009**, *261*, 88–93.
- (30) Sun, Z.; Yuan, H.; Liu, Z.; Han, B.; Zhang, X. *Adv. Mater.* **2005**, *17*, 2993–2997.
- (31) Qu, X.; Kobayashi, N.; Komatsu, T. *ACS Nano* **2010**, *4*, 1732–1738.
- (32) Kundu, S.; Huitink, D.; Liang, H. *J. Phys. Chem. C* **2010**, *114*, 7700–7709.
- (33) Kundu, S.; Liang, H. *Langmuir* **2010**, *26*, 6720–6727.
- (34) Yang, W.; Yang, C.; Sun, M.; Yang, F.; Ma, Y.; Zhang, Z.; Yang, X. *Talanta* **2009**, *78*, 557–564.
- (35) Zhang, J. L.; Wang, Y.; Ji, H.; Wei, Y. G.; Wu, N. Z.; Zuo, B. J.; Wang, Q. L. *J. Catal.* **2005**, *229*, 114–118.
- (36) Tayyari, S. F.; Milani-nejad, F. *Spectrochim. Acta, Part A* **2000**, *56*, 2679–2691.
- (37) Stabnikov, P. A.; Pervukhina, N. V.; Baidina, I. A.; Sheludyakova, L. A.; Borisov, S. V. *J. Struct. Chem.* **2007**, *48*, 186–192.
- (38) Menini, C.; Park, C.; Shin, E.; Tavoularis, G.; Keane, M. *Catal. Today* **2000**, *62*, 355–366.
- (39) Chon, S.; Allen, D. *ALChE J.* **1991**, *37*, 1730–1732.